RSC Advances

ROYAL SOCIETY OF CHEMISTRY

www.rsc.org/advances

Cite this: DOI: 10.1039/c0xx00000x

www.rsc.org/xxxxxx

ARTICLE TYPE

Regulable Switching from P- to N-type Behavior of Ordered Nanoporous Pt-SnO_2 Thin Films with the Enhanced Room Temperature Toluene Sensing Performance

Shaofeng Shao,*[a] Hongyan Wu,[a] Fan Jiang,[a] Shimin Wang,[a] Tao Wu,[a] Yating Lei,[a] Ralf Koehn,[b] and Wei-Feng Rao[a]

Received (in XXX, XXX) Xth XXXXXXXXX 20XX, Accepted Xth XXXXXXXXX 20XX
DOI: 10.1039/b000000x

Gas sensing with ordered nanoporous materials is achieving much attention because of its promising capability of detecting toxic gases at room temperature. In this work, an ordered nanoporous Pt-SnO_2 sensing film is fabricated in situ on a sensing device using a block polymer template and is applied as a chemiresistive toluene gas sensor. The post synthetic hydrothermal treatment was developed for the synthesis of the ordered Pt-SnO_2 sensing films with homogeneous and controlled film thickness and the controllable pore size. The structure, crystallinity and composition of the ordered nanoporous Pt-SnO_2 thin films are characterized by HRTEM, FESEM, SAED, and STEM. Interestingly, the Pt-SnO_2 nanoporous film, an n-type material, presents tunable sensing behaviour with the switching from p- to n-type toluene sensing performance as a function of the platinum content and calcination temperature. The ordered nanoporous sensing film is capable of detecting low levels of toluene, as low as 10 ppm, at room temperature, and shows good stability. Furthermore, a transition diagram has been created on the basis of the toluene sensing response, which can be used to design the p-n transitions.

.

1. Introduction

Chemical gas sensors have received much attention in science and are gaining importance in everyday life, because of their extensive applications in a variety of fields, such as food safety, medicine diagnosis, and citizen security.[1, 2] The most recent research in gas sensors has focused on highly sensitive sensors for the detection of toxic and detrimental gases. Among the harmful gases, toluene is harmful to human skin, mucous membrane and nervous system. Trace levels of toluene are sufficient to damage the human respiratory system and lung tissues.[3] In this regard, trace-level toluene detection and air quality monitoring are of great significance to public health and the environment. In far, a series of techniques have been developed to detect trace levels of toluene, including electrochemical, optical, and chemiresistive sensors.[3-8] Among these, chemiresistors based on semiconducting metal oxides (SMOs) have been indicated as the most promising materials, which can easily award sensors with irreplaceable merits of low cost, simple fabrication, direct electrical readout, and good compatibility with Si processes.[9, 10]

In recent years, the detect of trace levels of toluene has been reported using semiconducting metal oxide sensors based on a rich variety of nanostructures, such as nanoparticles, nanowires, nanoneedls, and nano-size films.[8, 11-13] Among these, ordered nanoporous metal oxides thin films have proved to be of great value in gas sensing applications.[14, 15] Ordered nanoporous structure leads to increased surface area, richer surface active sites, strong adsorption of the target gas molecules, and thereby to enhanced sensing performance. Kim et al. developed a nanoimprinting method for the fabrication of sensor device to produce the porous sensing film, which was able to detect VOCs vapour at room temperature. [16] However, the fabricated gas sensors presented poor sensing performance. In our previous studies, we have developed an efficient approach for synthesis of ordered crystalline nanoporous metal oxide such as post-synthetic water vapour hydrothermal treatment.[17] It allows the synthesis of metal oxide thin films with ordered nanopores at low temperature. Furthermore, crystalline pore walls can be achieved at low temperatures allowing an easy thermal removal of the template by calcination without significant shrinkage of the thin film normal to substrate. Therefore, the post-synthetic hydrothermal treatment would provide an effective way to research the effect mechanism of nanostructured ordering, nanopore size, and particle size of nanoporous metal oxides on their corresponding application property. However, the further application of metal oxide with post-synthetic hydrothermal treatment on gas sensor is necessary.

Crucial efforts have been concentrated to ameliorate the recognition ability of ordered metal oxide sensors, usually by doping or surface modification.[18, 19] Recently, the discovery of

transitions from p- to n-type gas sensing presents a new and promising way for gas discrimination.[14, 20-24] The n- or p-type gas sensing relates to the increase or decrease of sensor resistance upon exposure to an oxidizing gas. To date, the regulable transition of metal oxide materials sensing behaviour from p-type to n-type were induced by treatment in the operation temperature and the concentration of the reducing gas. For instance, Huang et al. [21] reported a ZnO-modified SnO_2 sensor revealing concentration-dependent n-p-n transitions in the sensing response to reducing gas; Wang et al. [25] exhibited temperature and concentration-dependent n-p transition performance in hydrothermally synthesized ZnO nanotube arrays. Dai et al. [14] synthesized a honeycomb-like Fe_2O_3 porous sensing film demonstrating abnormal sensing behaviour with reversible switching from p- to n-type NO_2 sensing tuned by the NO_2 concentration (C) and working temperature (T). However, the mechanism and controllability of such p-n transitions of SnO_2-based sensors at room temperature are rarely investigated and remain challenging to understand.

In this work, an ordered nanoporous Pt-SnO_2 sensing film is synthesized in situ on a sensing device using a block polymer template and is evaluated as a chemiresistive toluene gas sensor. The post synthetic hydrothermal treatment was developed for the synthesis of the ordered Pt-SnO_2 sensing films with homogeneous and controlled film thickness and the controllable pore size. The structure, crystallinity and composition of the ordered nanoporous Pt-SnO_2 thin films are characterized by HRTEM, FESEM, SAED, and STEM. Interestingly, the SnO_2 nanoporous film, an n-type material, demonstrates sensing behaviour with reversible switching from p- to n-type toluene sensing performance. Further, a transition diagram has been created on the basis of the toluene sensing responses, which can be used to design and tailor the p-n transitions.

2. Fabrication and measurement of sensors

2.1 Sensing Film Fabrication and Characterizations.

The Sn precursor solutions were prepared by dissolving 1 g $SnCl_4$ (Aldrich) in 0.16 mol ethanol in the presence of 4.0E-5 mol PluronicF127 triblock copolymer ([$(HO(CH_2CH_2O)_{106}$-$(CH_2CH(CH_3)O)_{70}$-$(CH_2CH_2O)_{106}H$, $EO_{106}PO_{70}EO_{106}$], Sigma). For Pt doping, 0.04g $PtCl_4$ (Aldrich) was dissolved in 1.0 ml 12 M HCl and then mixed with the above tin precursor solution under constant stirring for overnight. The resulting (clear) Pt-Sn precursor solutions were stable over a one month period. The molar ratio of $SnCl_4$:F127:EtOH:$PtCl_4$:H-Cl:H_2O in the final Pt-Sn precursor solution was 1:0.01:40:0.062:3:10. Gas sensing thin films were prepared by spin-coating 50 µl of the Pt-Sn precursor solution onto one sensor device of *ca*. 10 × 10 mm^2 with interdigital electrode at 4000 rpm for 60 s under 30% relative humidity for two times, and then dried at 60°C for 2 h. The films were then exposed to a water vapor hydrothermal treatment, 85% relative humidity, at 95°C for 96 h. The relative humidity was achieved using a supersaturated salt aqueous solution, kept at 95°C, in a humidity controlled chamber. The films were then heat treated by annealing at temperatures of 200, 300, 400 and 500°C for 2 h with an up/down ramp rate of 1.0°C/min.

SAXRD patterns of the thin films were taken on an XDS-2000 diffractometer (Scintag Inc.) using Cu K radiation. WAXRD data were obtained by a Bruker D8 Advance X-ray diffractometer with Cu Ka (0.15406 nm) radiation. Field-emission scanning electron microscopy (FE-SEM, Hitachi S-4800) was used to observe the morphologies of the sensing films. Nitrogen sorption measurements were carried out at 77 K using a NOVA 4000e (Quantachrome Instruments) on Pt doped tin oxides scratched from several films. High resolution transmission electron microscopy (HRTEM) and scanning transmission electron microscopy in high angle annular dark field mode (STEM-HAADF) were performed using a FEI Titan 80-300 equipped with a field emission gun operated at 300 kV; film parts were scratched from the substrate and collected on an amorphous holey carbon film on a copper grid. XPS spectra were recorded using a Kratos Axis Ultra DLD spectrometer employing a monochromated Al-Ka X-ray source (hv= 1486.6 eV), hybrid (magnetic/electrostatic) optics and a multi-channel plate and delay line detector (DLD). Surface charging was corrected by referencing the spectra to C-C state of the C 1s peak at binding energy at 284.6 eV. All XPS spectra were recorded using an aperture slot of 300*700 microns, survey spectra were recorded with a pass energy of 160 eV, and high resolution spectra with a pass energy of 40 eV.

2.2 Gas-Sensing Measurement

During the sensing measurement, liquid VOCs were inputted through a sample inlet and led down to a heater, which vaporized it. A fan ensured that the vapour was homogeneously distributed. The gas sensing properties were determined in a sample cell consists of a sample chamber and has a gas inlet and outlet. Resistance changes upon sample exposure to gases were recorded by a high resistance meter Keithley 6517A. The sensor response is defined as $S= (R_a-R_g)/R_g$ or$= (R_g-R_a)/R_a$, where R_a and R_g are the sensor resistances in air and in the target gas, respectively. Here, the response or recovery time is defined as the time taken for the sensor to achieve 90% of its maximum response or decreases to 10% of its maximum response, respectively.

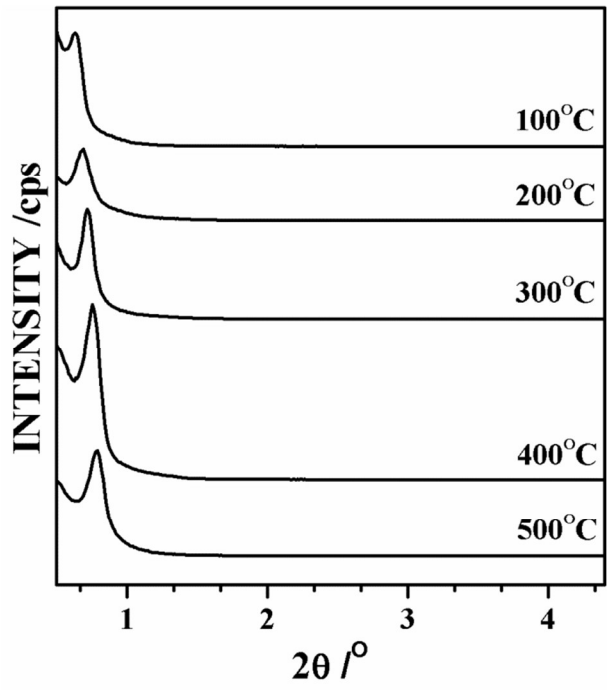

Fig. 1 Small-angle XRD patterns of nanoporous Pt-SnO_2 thin films synthesized after 95°C hydrothermal treatment and annealing at 100°C, 200°C, 300°C, 400°C and 500°C.

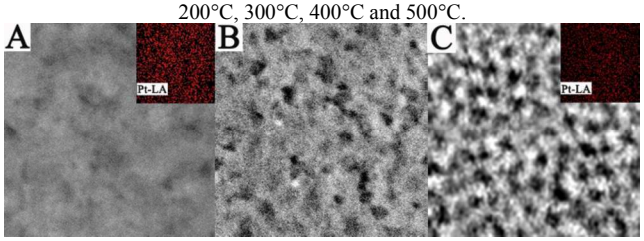

Fig. 2 (A), (B), and (C) FESEM images of the 200°C, 300°C, and 400°C annealed ordered nanoporous Pt-SnO_2 film. The top right insets of images A and C are EDX mapping analysis of Pt-LA;

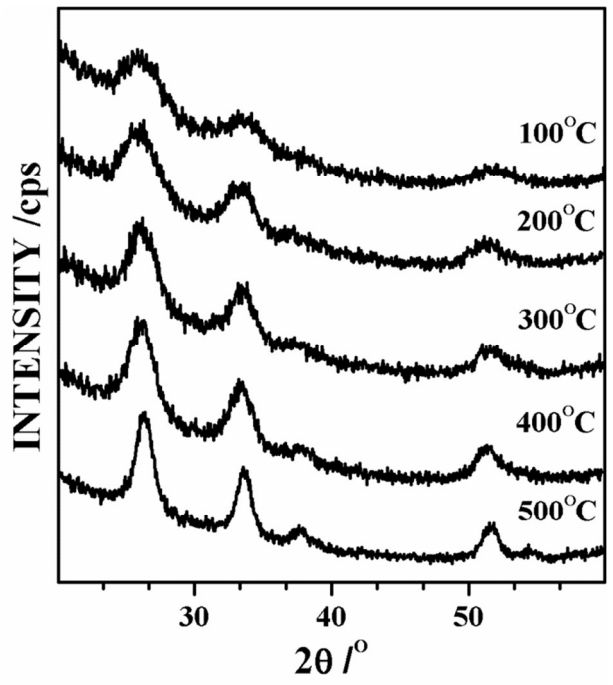

Fig.3 Wide-angle XRD patterns of nanoporous Pt-SnO_2 thin films synthesized after 95°C hydrothermal treatment and annealing at 100°C, 200°C, 300°C, 400°C and 500°C.

3. Results and discussion

In this work, the Pt-SnO_2 sensing films exhibited tunable sensing behaviour with switching from p- to n-type VOC sensing through the change of the calcination temperature and platinum element content. Therefore, the calcination process has great effect in the nanostructure ordering, particle size, and composite. The research aim of this work is to find the particular relation between the nanostructured ordering, particle size, and composite of ordered nanoporous SnO_2 and their gas sensing performance. For this purpose, as-synthesized sensing films were heat treated at different temperatures. The crystallinity and structure of the synthesized thin films were examined by X-ray diffraction. For the as-synthesized air-dried Pt-SnO_2 thin films, no diffraction peaks were observed within the small angle X-ray diffraction (SAXRD) patterns (not shown for brevity), indicating a disordered nanostructure. An ordered nanostructure formed after exposing the Pt-SnO_2 thin films to the hydrothermal treatment (95°C, 96 h) then being heat-treated at 100°C was indicated by the peak appearing at ≈ 0.63° on the SAXRD pattern, Fig. 1. The SAXRD patterns of the thin films of Pt doped SnO_2 heat-treated at different temperatures are depicted in Fig. 1: 200, 300, 400, and 500°C, respectively. The ordered nanostructure of the thin film is still retained through the progressive thermal treatment. When the calcination temperature increases from 200 to 400°C, the diffraction peaks become sharper and stronger, and then the diffraction peaks intensity decrease with further increase in the calcination temperature. Compared with the hydrothermal treated thin film, the pattern of the 400°C annealed film is much stronger indicating the excellent thermal stability of the ordered nanoporous structure. Since ordered nanoporous topologies are known to commonly collapse with annealing temperatures as low as 250°C, the described synthesis technique represents a significant advance in the ability to maintain the high temperature structural stability of such highly ordered nanoporous architectures.

Sinturel et al. [26] reported that the SVA process develops the synthesis of the block polymer thin films where the self-assembled pattern is used to create surface topography or chemical composition variation for application. However, the block polymer films produced at rapid solvent evaporation rates are "kinetically constrained" in a disordered arrangement. The post synthetic water vapour hydrothermal treatment in this work could solve the above problem. More importantly, this method allows us to construct ordered nanoporous architectures with different nanoparticle size and composition of the Pt on the film surface.

The calcination effect for the synthesis of Pt-SnO_2 with varied nanoporous ordering and surface composition can be clearly observed from the high resolution SEM images show in Fig. 2. When the calcination temperature is low, for example, 200°C, the pore size of sensing film is very small and the Pt content on the film is high, as shown in the insert image of Fig.2A, which introduces a tight connection between PtOx particles on the surface of sensing film. With the increase of calcination

temperature to 300°C, this leads to the formation of partly regular nanopores on the film surface. One can see that the 400°C calcined sensing film is highly ordered with regular nanopores. However, the Pt content of the sensing films drops dramatically from 12 at% to 3 at%. Thermogravimetry analysis was carried out not only to clarify the thermal stability of the scratched films with post synthetic hydrothermal treatment but also to determine the nature of the remaining template and the calcination temperature required to eliminate the template. The TG curve depicted in ESI, Fig. S1 shows the change in the mass of the scratched films between 40 and 800 °C under an air flow. The TG curve presents the mass loss occurring in two main successive steps of 12.4 (centered at 184.5°C) and 9.1(centered at 225.5°C) to give a final residue of 78.5%. Moreover, no significant weight loss is detected above 350°C, indicating that organic templates are eliminated at this temperature. As a consequence, the first decomposition step can be attributed to the elimination of adsorbed water, whereas the main step at higher temperature (225.5°C) is related to the thermal degradation of the organic template. The results are in good agreement with the SEM measurement.

XRD patterns of heat-treated Pt-doped SnO_2 sensing films are shown in Fig. 3. The peak position and relative intensity of all diffraction peaks for the products match standard powder diffraction data (JCPDS 41-1445). The XRD patterns of 100°C heat-treated Pt-SnO_2 thin films exhibits three discrete *hkl* reflection at 26.6°, 33.9°, and 51.8°, respectively, corresponding to the (110), (101), and (211) crystallographic planes of tetragonal SnO_2 in accordance with the synthetic cassiterite. All diffraction peaks in Fig. 3 became stronger and sharper with the higher heat treatments. When the calcination temperature is up to 400°C, the XRD patterns of sensing films exhibits five discrete *hkl* reflection at 26.6°, 33.9°, 38.0°, 51.8°, and 54.8°, respectively, corresponding to the (110), (101), (200), (211) and (220) crystallographic planes of tetragonal SnO_2. No characteristic peaks belonging to other SnO_2 crystals or impurities were detected. The average crystalline grain size (D) calculated from the full width at half-maximum, FWHM, of the (110) reflection line using the Scherrer formula, [The average crystallite size (Ds) was abtained by $Ds=0.9*\lambda/(B*\cos\theta)$, where λ is the wavelength of X-ray ($\lambda_{Cu}=0.15418nm$) and B is the full-width at half-maximum of the XRD peak centered at 2θ degrees], is 1.6 nm for the 100°C heat-treated Pt-SnO_2 thin film, 2.4 nm for the 200°C heat-treated thin film, 3.0 nm for the 300°C heat-treated thin film, 3.8 nm for the 400°C heat-treated thin film, and 5.2 nm for the 500°C heat-treated thin film. However, peaks of Pt phase cannot be seen in these patterns due to possibly to the absence of crystalline PtO_x aggregated particles.

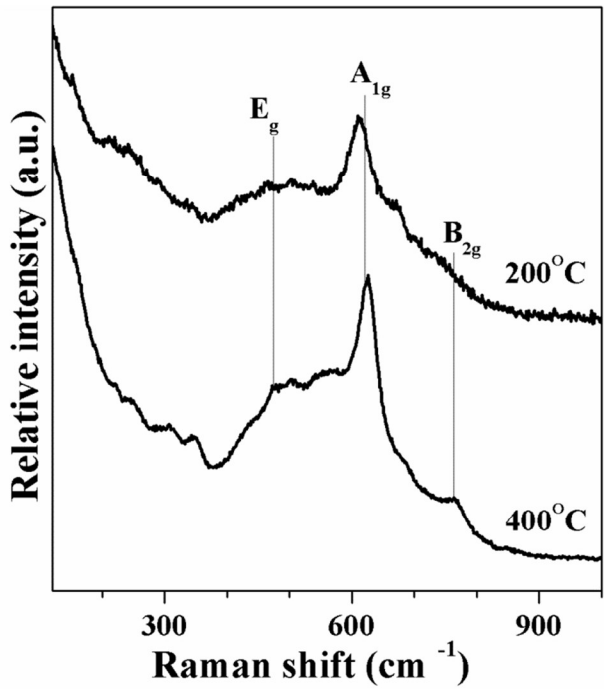

Fig.4 shows Raman spectrum of 200°C and 400°C heat-treated sensing film.

Fig. 4 shows the evolution of Raman spectra versus the treatment temperature for Pt doped SnO_2 sensing films. Spectra of 200°C heat-treated sensing film exhibits around the A_{1g} mode a broad feature attributed to surface modes,[27] whereas the Raman bands measured at 212, 235, and 344 cm^{-1} were not detected in the bulk SnO_2. Liu et al.[28] have reported, besides the expected E_g and A_{1g} bands, Raman bands located at 212 and 235 cm^{-1} in SnO_2 nanomaterials, which were attributed to E_u (TO) and E_u (LO) active modes. It is reasonable to assign the two volume modes to IR modes whose Raman activities are induced by the size effect, which are due to the smaller diameter of SnO_2 nanoparticles. The third broad peak at 344 cm^{-1} is also due to an active mode from the inactive E_u mode. This attributes to relaxation of Raman selection rule by reduction the particle size to several nanometers, also by the high concentration of defects in surface site such as oxygen vancancies (VOs) and lattice disorder. [29] The other peculiarity of Raman spectra of nanocrystalline SnO_2 is the broad feature between 400 and 700 cm^{-1}, called band of the surface modes. The origin of these bands has been connected to the low particle dimension of the materials. Dieguez et al. [30] proposed that surface modes were due to the existence of a lattice softening taking place in the outer part of the grain. On the other hand, studies of nanocrystalline tin oxide reactivity have shown that the relative intensity of surface bands depends strongly on the interactions with gases, which can modify the outer layer of the gain.[31] For 400°C heat-treated sensing film, the three detectable Raman active modes of tin oxide have been observed: E_g (476cm^{-1}), A_{1g} (627cm^{-1}), and B_{2g} (766cm^{-1}). Two other bands are observed at 241, and 288 cm^{-1}, together with broad feature located at the region 310-350 cm^{-1} due to the particle size increase during the calcination process. It corroborates that the calcination process has significantly influence on the nanostructure of the materials, especially on the surface modes.

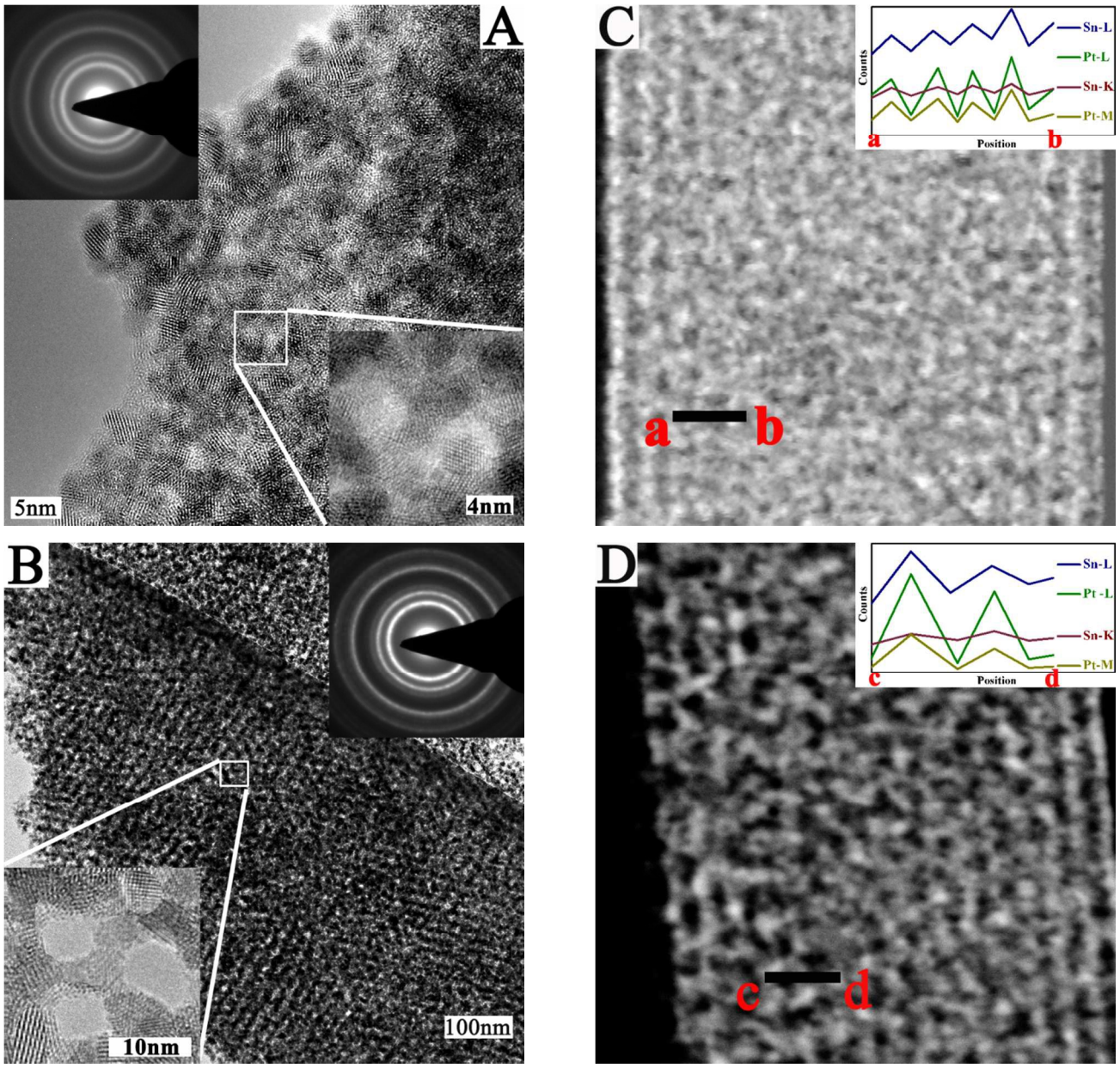

Fig.5 (A) TEM image of 300°C annealed sensing film. The top left inset shows SAED pattern of displayed area indicating the polycrystalline nature of the film. The bottom right inset is the HRTEM image of the rectangular marked region; (B) TEM image of 400°C annealed ordered nanoporous Pt-SnO_2 film. The top right inset shows SAED pattern of displayed area indicating the polycrystalline nature of the film. The bottom left inset is the HRTEM image of the rectangular marked region; (C) Cross-section scanning transmission electron microscopy image of the 200°C annealed Pt-SnO_2 sensing film. The inset shows energy dispersive X-ray scattering (EDX) line measurement taken through a black line ab showing the presence of Pt, Sn; (D) Cross-section scanning transmission electron microscopy image of the 400°C annealed Pt-SnO_2 sensing film. The inset shows energy dispersive X-ray scattering (EDX) line measurement taken through a black line cd showing the presence of Pt, Sn.

As shown in ESI, Fig. S2, the interdigitated-finger arrays on the sensor device are clearly observed; the electrodes contain twenty fingers. Each finger is 10μm in width and 1mm in length, finger-finger spacing is 8μm, with a finger-to-finger overlap of 800μm. Fig. 5A is a high resolution transmission electron

microscope (HRTEM, TITAN 80-300) image of a 200 °C heat-treated thin film showing crystalline nanocrystals with the selected area electron diffraction (SAED) pattern (Fig. 5A, inset) displaying clear diffraction rings assignable to (110), (101), and (211) crystallographic planes of tetragonal SnO_2 in accordance with the synthetic cassiterite. The high-magnification image of the selected area in insert image of Fig. 5A presents the walls of the porous inorganic framework consisting of crystallized tin dioxide grains, where the nanopores are packed in an arrangement with an average pore size of approximately 2-3 nm. Fig. 5B shows a TEM image of a 400 °C annealed nanoporous film; the nanopore arrays are packed in an ordered arrangement with a repeating distance. The difference between the pore sizes of both films is quite clearly observed from the high-magnification insert images of Fig. 5A and 5B. For the 400 °C annealed nanoporous film, the nanopore arrays are packed in an ordered arrangement with an average pore size of approximately 7-8 nm. To gain more insight about the distribution of platinum, STEM observation was carried out. STEM images, in high-angle annular dark-field mode, travelling over film cross-sections-see Fig. 5C and D -reveal the dispersion of the platinum within the ordered nanoporous films. Further EDX line measurements taken from the selected area (marked by a black line in Fig 5C and 5D) exhibit the presence of platinum and tin, indicating that the 200°C heat-treated sensing film with high content of Pt and small pore size forms much more PtO_x/SnO_2 heterojunctions than that of the 400°C heat-treated sensing film with low content of Pt and bigger pore size. Therefore, for 200°C calcined thin films, the PtO_x/SnO_2 heterojunctions would play more importance role in sensing films' gas-sensing properties at room temperature. However, it is impossible to discriminate platinum with tin dioxide for both two films, indicating the nice dispersion of platinum all over the two films.

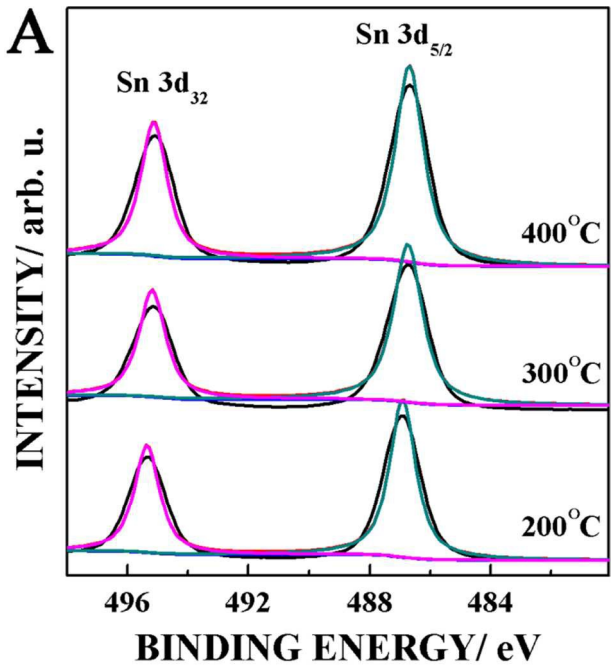

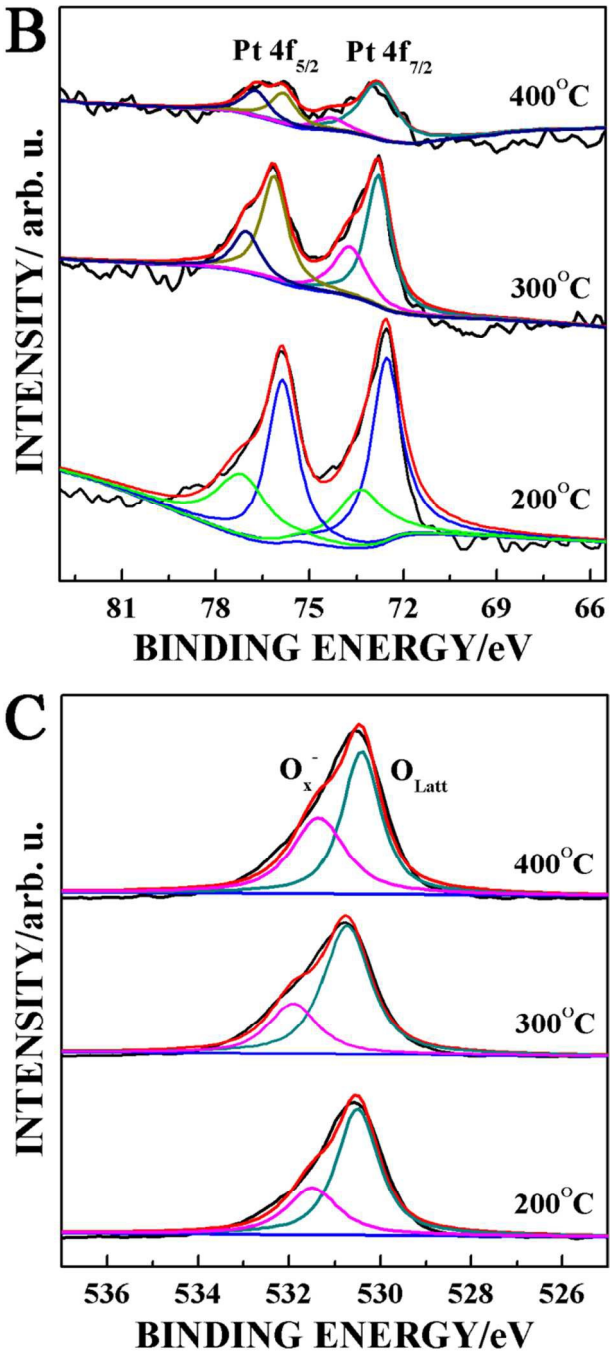

Fig.6 (A) Sn 3d, (B) Pt 4f and (C) O 1s spectra of the 200°C, 300°C and 400°C annealed ordered nanoporous Pt-SnO_2 film.

To get deeper insights in the chemical composition of thin films surface, Pt-doped SnO_2 thin films heat-treated at different temperature ranging from 200 to 400°C were studied by XPS and the representative high-resolution XPS spectra comprising Sn3d, Pt4f, and O1s core levels of Pt-doped SnO_2 sensing film after different heat treatment, show in Fig. 6. The Sn 3d core level spectra of the 200°C heated Pt-doped thin films shown in Fig. 6A consists of a doublet located a binding energies of 486.9 and 495.4 eV, which can be assigned to the Sn $3d_{5/2}$ and Sn $3d_{3/2}$ of Sn^{4+} in SnO_2, respectively. The splitting of the 3d doublet is 8.5 eV, demonstrating that the Sn in the thin films is in a single form

of Sn^{4+}. Analysis of the Sn 3d core level spectrum of the 400°C heated Pt-doped thin films displays a binding energy shift of +0.2 eV compared to the 200°C heated thin films.

In Fig. 6B, the Pt 4f core level line of the 200°C heated Pt-doped thin films could be fitted with two main doublets with E_b of Pt $4f_{7/2}$ at 72.5eV and 73.5 eV. The platinum state with the lower E_b can be assigned to Pt^{2+} in platinum oxide (PtO) but with shift to a lower energy by 0.6 eV in relation to the E_b of bulk PtO, which was expected to smaller oxidized platinum nanoparticles than in case of the bulk oxide. The Pt $4f_{7/2}$ peak with the higher E_b can be assigned to the strong oxidized platinum (4+) state. PtO_2 is unstable in its anhydrous form but has been shown to be stabilized by the matrix of other oxides, such as SnO_2 and PtO. Therefore, it is reasonable to propose that the Pt^{4+} state in our work is stabilized in its anhydrous form by the SnO_2 oxide. On the other hand, the Pt 4f peak shows a positive shift of ~0.3 eV from the 200°C heat-treated thin films to 400°C treated thin films. The energy shift with increasing calcination temperature is a result of the growth of PtO_x nanoparticles, which introduces more Pt atoms progressively away from the interface with the SnO_2 particles and thus results in a weaker electronic interaction between the Pt atoms and the SnO_2 thin film. Furthermore, the peak intensity of Pt Eb dramatically decreases with the temperature increase from 200°C to 400°C, which is in good agreement with the SEM studies. The significant changes of nanoporous ordering, surface composition, and electronic interaction can greatly influence the sensing behaviour of the SnO_2 thin film. Because PtO exhibits the p-type semiconductor property with a band gap of 0.86 eV, as opposed to the n-type SnO_2 (3.6 eV), Oxidized PtO_x can create p-n junctions on the large surface area of ordered SnO_2 thin films. For 200°C calcined thin films, the PtO_x/SnO_2 heterojunctions play an importance role here. The adsorption of oxygen on the surface may full deplete the electrons in the PtO_x layer as the thickness of PtO_x is smaller than the Debye length (ca. 3nm). A depletion zone where PtO_x has penetrated into the SnO_2 films is formed. In addition, Pt cations work as acceptor dopants in n-type SnO_2. Consequently, together with the synergetic depletion effect, the dominant carriers in the PtO_x/SnO_2 interface layer change from electrons to holes. As one can expect, the conduction type of the thin films will be p-type. For 400°C calcined thin films possess highly ordered nanopores with high size, the low content of oxidized Pt nanoparticles, the sensor undergoes a transition from p- to n-type with increasing calcination temperature, which can be explained by the surface-depletion model. When the ordered nanoporous sensing film is exposed to dry air, oxygen ions are adsorbed onto the inner and outer surface of the sensing films. Therefore, the depletion layer may extend throughout the whole area of the sensing films nanostructure. Therefore, the resistance increases and the sensor response inverts to n-type.

The high-resolution XPS spectrum of O1s for the 200°C heated Pt-doped thin films is shown in Fig. 6C, one finds that the O1s consists of two components in different chemical states: O_{latt} (530.78 eV) and O_x^- (531.88eV). O_{latt} is attributed to the oxygen ions in the crystal lattice which are thought to be pretty stable and have no contribution to the gas response, meanwhile, O_x^- is attributed to the adsorbed oxygen ions, which have a very important role in the gas sensing property and will be further discussed in the sensing mechanism section, in the oxygen deficient regions such as oxygen vacancy (V_o), oxygen interstitial (O_i) and oxygen antisite (O_{sn}) defects.[32] With the increase of calcination temperature up to 400°C, the intensity of O_x^- increases significantly as well as, which supports the surface-depletion model brought up above to some degree.

Gas-sensing Characteristics

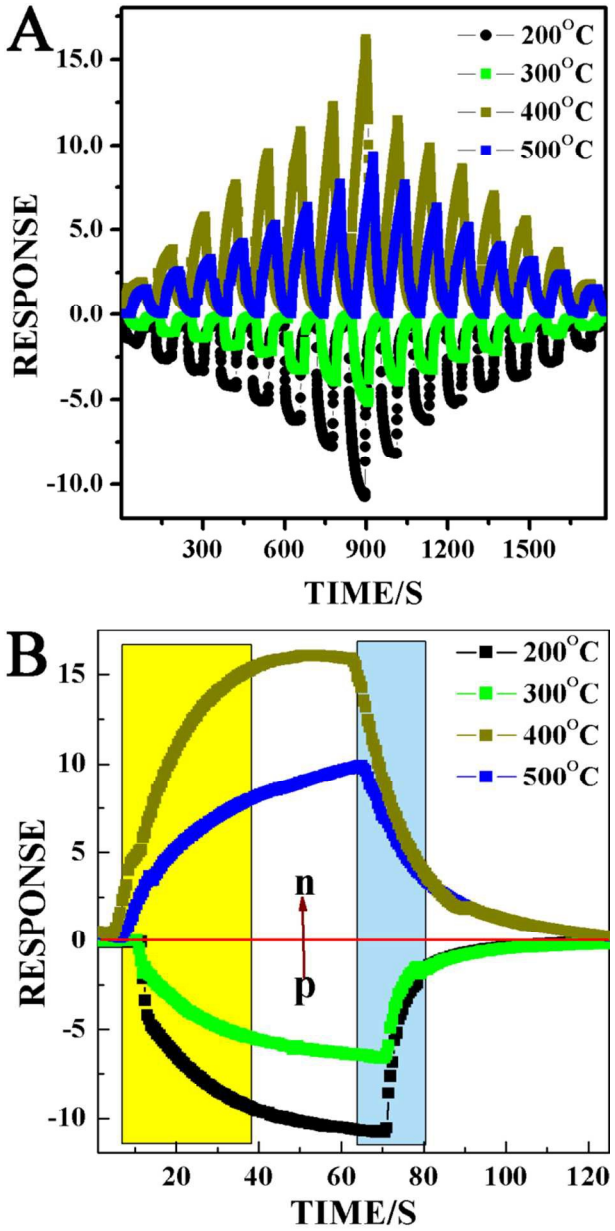

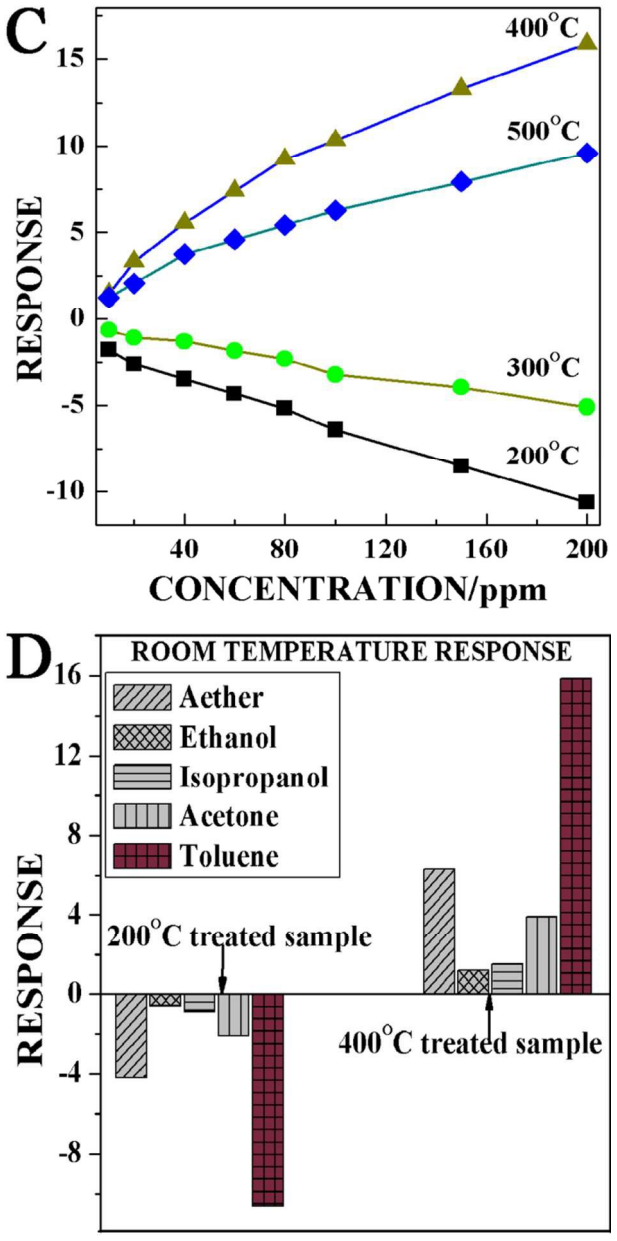

Fig.7 (A) Response curves of 200°C (12 at% Pt), 300°C (6 at% Pt) and 400°C (3 at% Pt) annealed ordered nanoporous Pt-SnO_2 film sensors measured under various toluene gas concentrations; (B) Typical response and recovery curves of the 200°C (12 at% Pt), 300°C (6 at% Pt) and 400°C (3 at% Pt) annealed ordered nanoporous Pt-SnO_2 film sensors to toluene gas at 200 ppm; (C) Normalized response of the 200°C (12 at% Pt), 300°C (6 at% Pt) and 400°C (3 at% Pt) annealed ordered nanoporous Pt-SnO_2 film sensors as a function of toluene gas concentrations; (D) Selectivity histograms of sensor responses to 200 ppm of toluene, isopropanol, ethanol, aether, and acetone vapour of 200°C (12 at% Pt), 300°C (6 at% Pt) and 400°C (3 at% Pt) annealed ordered nanoporous Pt-SnO_2 film sensors at room temperature.

The structure and morphology of metal oxide materials were reported to have a large effect on their physical, chemical, and application performance. In this work, the ordered nanoporous structure and particle size control of SnO_2 are realized by the improved post hydrothermal treatment, which is expected to bring about more efficient gas sensing performance as compared to conventionally prepared SnO_2 sensing films. On the other hand, metal element doping has also long been proven to be a facile and efficient way to enhance the sensing property of semiconductor metal oxide sensors, because doping can effectively modulate the parameters of the crystal cell and the adsorption of oxygen. In this work, we researched the platinum element doping effect on sensing films' gas-sensing properties at room temperature after different calcination process.

In this study, the sensor response is defined as $\Delta R/R$, where ΔR stands for the resistance variation (R_a-R_g). This parameter is positive (negative) for n-type (p-type) toluene sensing. Pristine nanoporous SnO_2 thin films showed the R_{air} value of 70MΩ while the 200°C heated Pt-doped SnO_2 thin films had a more than two-fold higher R_{air} (150 MΩ) probably due to the extended electron depleted regions arising from oxygen adsorption on the thin film. The ordered Pt-doped nanoporous thin films showed a dramatic increase in R_{air} compared to the pure SnO_2 thin films. This result might be attributed to the formation of depletion layers from p-n junctions between p-type PtO and n-type SnO_2. The measurement were performed at room temperature with toluene gas exposure concentration ranging from 10 ppm to 200 ppm, and the test were switched from low concentration to high concentration, and then conversely from high concentration to low concentration. However, an abnormal resistance increase occurs on exposure to toluene vapour. Chemiresistive sensors are classified as n or p type depending on whether their conductance increases or decreases when they are exposed to a reducing gas, and vice versa for oxidizing gases, i.e. decreased conductance is expected for n-type sensing. In this context, the 200°C and 300°C heated sensing films exhibit an unusual p-type gas sensing response to toluene, more like that of a p-type metal oxide, as shown in Fig. 7A.[14] Each exposure/recovery cycle were carried out for an exposure interval of 50 sec followed by a recovery interval of 50 sec in dry air. The sensor response clearly tracks the change in the toluene concentration. Moreover, the responses are extremely fast, and the sensor can fully recover in very short times after toluene removal. Specifically, the response times, defined as the time necessary to reach 90% of the maximum response, range between 30 and 35 sec and decrease as the toluene concentration is increased. The recovery times are in the range of 15-20 sec and decreased as the toluene concentration decreased. However, it can be seen that the 200°C heated 12 at% Pt-SnO_2 sample is more sensitive than the 300°C heated 6at% Pt-SnO_2 sample. Taking 200ppm as an example, the 200°C heated Pt-SnO_2 sample exhibits a sensitivity of 10.5, which is higher than that (5.4) of the 300°C heated Pt-SnO_2 sample, as shown in Fig. 7B. One probable reason is that toluene reacted mainly at the PtO_x/SnO_2 interface layer. With the higher calcination temperature, the interface layer has been partly collapsed during the increase of the number and size of nanopores, which is in good agreement with the FESEM results. Therefore, the catalytic activity of PtO_x becomes weaker and the change of the resistance in the 300°C heated Pt-SnO_2 sample will be lower than that of the 200°C heated Pt-SnO_2 sample. The above results are in good agreement with the report that the general nature of this phenomenon related to the behaviour of semiconductor surfaces itself, the formation of p-type conductivity on n-type semiconductor can be caused by a formation of an inversion layer at the surface and therefore to the inversion of the type of mobile carrier at the surface.[33] As calcination temperatures increased to 400°C, Pt-doped SnO_2 thin

films possess highly ordered nanopores with high size, the lowest content (3at%)of oxidized Pt nanoparticles. When the ordered nanoporous sensing film is exposed to dry air, oxygen ions are adsorbed onto the inner and outer surface of the sensing films. Therefore, the depletion layer may extend throughout the whole area of the sensing films nanostructure. Upon exposure to toluene, the ordered nanoporous sensing film quickly responds with a decrease in resistance, which reveals the typical n-type semiconducting behaviour of sensing films. A clear increase in the sensitivity is observed with the increasing gas concentration, and of all the materials tested, ordered nanoporous Pt-SnO_2 sensing film after 400°C calcination exhibits the best toluene-sensing performance at room temperature, with high response to toluene concentrations between 10 and 200 ppm. For 200ppm toluene vapour, the 400°C heated Pt-SnO_2 sample exhibits a sensitivity of 15.9, which is higher than that (10.5) of the 200°C heated Pt-SnO_2 sample. Specifically, the response time, defined as the time necessary to reach 90% of the maximum response, range between 25 and 30 sec and decrease as the toluene concentration is increased. The recovery time is in the range of 13-17 sec and decreased as the toluene concentration decreased, as shown in Fig. 7B. With further increase of calcination temperature, the 500°C heated sensing film's toluene response reduces substantially compared with the optimal one, as shown in Fig. 7C. The unfavourable characteristic may be caused by the decrease of surface areas from 109.2 to 92.4 $m^2 g^{-1}$ (as shown in ESI, Fig. S3) and the nanoparticle size increase from 3.8 to 5.2 nm. It should also be pointed out that ordered nanoporous 3at% Pt-SnO_2 sample also possesses superior performance when compared with other SnO_2-based samples reported in previous works[4, 34], which means that post-synthetic hydrothermal treatment is an effective method to synthesize high sensitivity ordered nanoporous SnO_2 gas sensor. A similar sensitivity could not be observed in the case of a similar nanoporous tin dioxide thin film prepared under similar conditions but without platinum.

Selectivity is another very important parameter for the ordered nanoporous SnO_2 gas sensor, because poor selectivity will induce mistaken alarm and limit its extensive utilization. Several vapour organic compounds were tested to explore the potential application of Pt-doped nanoporous SnO_2 as an excellent sensor in terms of high sensitivity and fast response for chemical vapour detection at room temperature. The responses of the 200°C heated Pt-SnO_2 sample with 12 at% Pt and the 400°C heated Pt-SnO_2 sample with 3 at% Pt to five target gases with 200 ppm concentration at room temperature were further investigated, and the relevant results are shown in Fig. 7D. For both above two samples, the responses to toluene are much higher than that to aether, ethanol, isopropanol, and acetone, indicating the significant enhancement of the toluene selectivity with the platinum dopant. That is to say, the present sensors display quite outstanding selectivity to toluene, especially the 3 at% Pt-doped SnO_2, of which the responses reach 6.3, 1.2, 1.5, and 3.9 to aether, ethanol, isopropanol, and acetone, respectively. Thus, 3 at% Pt-doped SnO_2 sensing film exhibits not only high response but also high toluene selectivity against acetone and other gases at a low gas concentration of 200 ppm. It is important to note that high response to toluene of 3 at% Pt-doped SnO_2 sensing films based sensors is possibly due to more effective dissociation between Pt nanoparticles and the C_7H_8 gas than the other tested gases. C_7H_8, among the gases tested, is unique since it has an additional methyl group (-CH_3). This group plays a crucial role in enhancing the selectivity of sensors. The adsorption of C_7H_8 onto the Pt surface is significantly affected by electronic effects, which lower the barrier for adsorption of C_7H_8 by making the donation of electrons from the πCH_3 level to the Fermi level easier and by the making back-donation from the Fermi level to the πCH_3* level more facile.[35] However, at higher Pt doping levels (12 at% Pt in 200°C heated Pt-SnO_2 sample), the toluene response switch from n- to p-type. This characteristic may be caused by the high-level surface disorder on sensing films surfaces induced by the heavy Pt doping. The surface disorder can be represented as defective surface states that trap charge carries, causing pinning of Fermi-level. Therefore, the transition from n- to p-type conductivity on n-type semiconductor can be caused by a formation of an p-Pt-O-Sn layer at the surface and therefore to the inversion of the type of mobile carrier at the surface, which is in good agreement with the STEM results.[33]

Transition mechanism

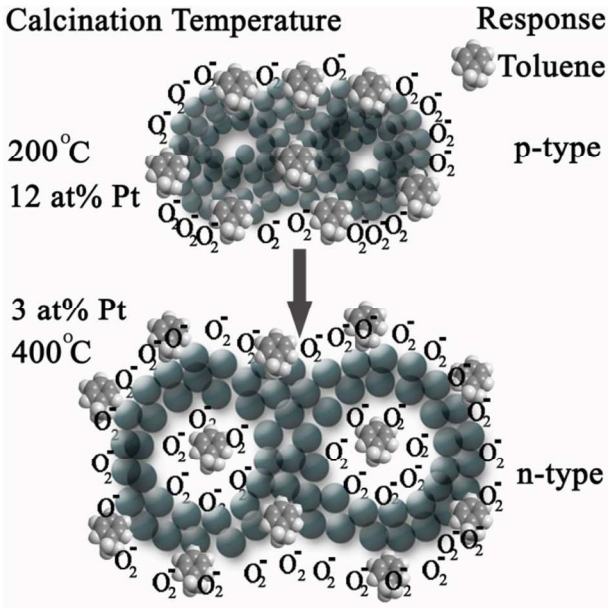

Scheme 1 Response mechanism of ordered nanopore and pore wall exposed to reducing gases or air.

The domination of electrons and holes, that is, n- or p- type nature, inside the functional metal oxide is of fatal significance in the application of gas sensing nanodevices. In general, n-type metal oxide nanomaterials are shaped due to oxygen deficiencies (vacancies), which lead to a donor level below but close to the conduction band. By comparison, p-type sensing behaviour is difficult to obtain except in cases where the material is naturally p type. The common avenue to synthesize the p type nanomaterials is through diffusion during the growth process or implantation into an as-grown sample, followed by post-treating at high temperatures in order to remove defects. There are some reports in the literature on the change of sensing response from n to p-type behaviour and vice versa. Gurlo *et al.* attributed the n-p switching of n-type α-Fe_2O_3 and In_2O_3-Fe_2O_3 sensors to an electronic origin.[36] Wang *et al.* attributed the concentration-dependent n-p transition observed in ZnO nanotubes sensors for

NO_2 gas to the co-existence of p-type and n-type ZnO nanotubes.[25] Lee *et al*. used a reductive ambient to obtain the direct transition between the n and p types of a metal oxide through a change of dominant carriers on the surface, namely, those of electrons or holes. [24]The calcination-dependent p-n transit of the sensing response to VOCs observed in the Pt-doped SnO_2 thin film sensors at room temperature has not been reported before. [21] The origin of this behaviour is as yet unclear but probably results from the surface chemistry of this system.

Doping SnO_2 with lower valency cations, such as Pt^{2+}, increases the Debye length by means of a decrease in the carrier concentration, which increases the films resistivity. Since Pt^{2+} acts as an acceptor type impurity, this could be expressed as:

SnO_2 -----Sn-O-Pt+O_0

O_0------V_0 + 2O_i

Where Sn-O-Pt is Pt substitution in Sn sites, O_0 represents lattice oxygen, V_0 represents lattice oxygen vacancies and O_i represents interstitial oxygen. Therefore, the elimination of electrons (increase in resistivity) can be expressed as:[20]

V_o---V_0^- + h^+

Based on the mechanism concerning surface band bending, [37] adsorption effects are expected to be quite significant in Pt-doped SnO_2 thin film-based sensor. PtO is a p-type semiconductor and it can form Schottky contacts with SnO_2 nanoparticles inducing a depletion layer in the SnO_2 thin film. According to the oxygen ionosorption model, oxygen is molecularly adsorbed on the PtO layer in the form of superoxide anions (O_2^-). The negative charges on the surface of SnO_2 would form surface band bending. Upon being exposed to toluene vapour, O_2^- forms will change into O^- or even O^{2-} forms via the Pt-catalyzed reactions. That is to say, when the 200°C heat-treated sensing film with high content of PtO and small pore size exposes to toluene vapour, toluene incorporation into PtO and SnO_2 semiconductors can form shallow donors. The contributed electrons by toluene incorporation are migrated to the sensing films and are restricted by the p-Pt-O-Sn layer. The band bends upward more dominantly, which results in the p-type behaviour at room temperature. Therefore, we are convinced that the p-n transit of the sensing response to toluene is closely associated with the Pt dopant, and the PtO_x/SnO_2 heterojunctions remain important to sensing properties of sensing films. Because of the close comparability in the work function of SnO_2 and PtO_x, charge transfer can readily proceed between them across the low interface barrier. The adsorption of oxygen on the surface may fully deplete the electrons in the PtO_x layer of the 200°C heat-treated sensing film as the thickness of PtO_x is smaller than the Debye length (ca. 3nm). A depletion zone where PtO_x has dispersed into the SnO_2 thin films is arranged. In addition, Pt cations reveal an evident tendency for the incorporation into Sn sites and work as acceptor dopants in n-type SnO_2. Thus, the hole concentration at the surface enhances by way of the diffusion and substitution of Sn^{4+} ions by Pt cations. Accordingly, together with the synergetic depletion effect, the dominant carriers in the Pt-O-Sn interface layer change from electrons to holes, thus p-Pt-O-Sn heterojunctions are formed. The sensors calcined at the temperature range of 100-300°C shows the p-type response to toluene at room temperature. With increasing calcination temperature, the dominant hole carrier concentration in the depleting layer and p-Pt-O-Sn layer decrease. By further increasing the calcination temperature to 400°C, the decreasing concentration of Pt on the p-Pt-O-Sn layer would reduce the band gap, which could decrease the junction barrier between the p-n interfaces. As one can expect, the conduction type will transit from p-type to n-type when the resultant electron concentration is in excess of the hole concentration with continuous increase of calcination temperature.[21] When the ordered nanoporous sensing film after 400°C calcination is exposed to dry air, oxygen ions are adsorbed onto the inner and outer surface of the sensing films. Therefore, the depletion layer may extend throughout the whole area of the sensing films nanostructure. On the other hands, upon exposure to reducing gas such as toluene, gas molecules will react with more concentration of chemisorbed oxygen ions at inner and outer surface of sensing films, as shown in Scheme 1. This increases the electrons concentration in the sensing film pore walls and narrows the surface depletion layer width, which leads to decrease in the resistance of ordered nanoporous sensing films. Hong and co-workers reported that the switching of sensing behaviour from p-type to n-type depended on deposition amount for SnO_2-SWNT[38] and ZnO-SWNT[39] hybrid sensors. When deposition amount of SnO_2 or ZnO on the surface of SWNT increasing, the sensing behaviour of hybrid sensors can be changed from p-type to n-type. Because the deposition amount of SnO_2 or ZnO increases in the hybrid sensors, the dominant charge carriers changes from holes to electrons in the sensors. For our work, when the sensing film with high content of platinum and small pore size exposes to toluene vapour, the contributed electrons by toluene incorporation are migrated to the sensing films and are restricted by the p-Pt-O-Sn layer. The band bends upward more dominantly, which results in the p-type behaviour at room temperature. The decreasing concentration of Pt on the p-Pt-O-Sn layer would reduce the band gap, which could decrease the junction barrier between the p-n interfaces. Therefore, when the sensing film with low content of platinum and larger pore size exposes to toluene vapour, the sensing behaviour will transit from p-type to n-type.

4. Conclusions

In this work, an ordered nanoporous Pt-SnO_2 sensing film is synthesized in situ on a sensing device using a block polymer template and is evaluated as a chemiresistive toluene gas sensor. The post synthetic hydrothermal treatment was developed for the synthesis of the ordered Pt-SnO_2 sensing films with homogeneous and controlled film thickness and the controllable pore size. The structure, crystallinity and composition of the ordered nanoporous Pt-SnO_2 thin films are characterized by HRTEM, FESEM, SAED, and STEM. Interestingly, the SnO_2 nanoporous film, an n-type material, demonstrates abnormal sensing behaviour with the switching from p- to n-type toluene sensing performance at room temperature as a function of the platinum content and calcination temperature. The ordered nanporous sensing film is capable of detecting low levels of toluene, as low as 10 ppm, at room temperature, and shows good stability. The best results with respect to porosity, nanostructural ordering, as well as the sensing behaviour are obtained by the tin dioxide thin films doped with 3 at% platinum prepared with spin-coating at 30% relative humidity, aging for 2 h at 60°C, for 96 h at 95°C and 85%

relative humidity and gradual calcination at 400°C. The toluene response of the SnO_2 sensing film with 3 at% Pt-doping level is found to be substantially improved up to 15.9 at 200 ppm with a short response time of ~25 s at room temperature. Furthermore, a transition diagram has been created on the basis of the toluene sensing responses, which can be used to design the p-n transitions.

Acknowledgments

This work was supported by the Startup Foundation for Introducing Talent of NUIST, National Natural Science Foundation of China (No. 51405242), and the grant of Specially-Appointed Professor of Jiangsu. We thank the Siemens AG for the helping in the design, preparation and donation of the sensor devices. We thank the University of Munich and especially Prof. Dr. T. Bein for his constant support.

Notes and references

[a] *Department of Materials Physics, School of Physics and Optoelectronic Engineering, Nanjing University of Information Science &Technology, Nanjing, China. Fax: +86-025-58731031; Tel: +86-025-58731031; E-mail: ssfshao@nuist.edu.cn*

[b] *Department of Chemistry & Biochemistry, University of Munich, Munich, Germany.*

† Electronic Supplementary Information (ESI) available: [details of any supplementary information available should be included here]. See DOI: 10.1039/b000000x/

Reference

1. A. Modi, N. Koratkar, E. Lass, B. Q. Wei and P. M. Ajayan, *Nature*, 2003, **424**, 171.
2. J. Kong, N. R. Franklin, C. W. Zhou, M. G. Chapline, S. Peng, K. J. Cho and H. J. Dai, *Science*, 2000, **287**, 622.
3. Y. Qu, H. Wang, H. Chen, J. Xiao, Z. Lin and K. Dai, *RSC Adv.*, 2015, **5**, 16446.
4. H. Shan, C. Liu, L. Liu, J. Zhang, H. Li, Z. Liu, X. Zhang, X. Bo and X. Chi, *ACS Appl. Mater. Interfaces*, 2013, **5**, 6376.
5. K. Suematsu, Y. Shin, Z. Hua, K. Yoshida, M. Yuasa, T. Kida and K. Shimanoe, *ACS Appl. Mater. Interfaces*, 2014, **6**, 5319.
6. J. Tian, J. Wang, Y. Hao, H. Du and X. Li, *Sens. Actuators, B*, 2014, **202**, 795.
7. S. Liu, Z. Wang, H. Zhao, T. Fei and T. Zhang, *Sens. Actuators, B*, 2014, **197**, 342.
8. S. Vallejos, I. Gracia, E. Figueras and C. Cane, *ACS Appl. Mater. Interfaces*, 2015.
9. M. E. Franke, T. J. Koplin and U. Simon, *Small*, 2006, **2**, 36.
10. K. Potje-Kamloth, *Chem. Rev.*, 2008, **108**, 367.
11. S. J. Hwang, K. I. Choi, J. W. Yoon, Y. C. Kang and J. H. Lee, *Chem. Eur. J.*, 2015, **21**, 5872.
12. M. Mori, Y. Itagaki, J. Iseda, Y. Sadaoka, T. Ueda, H. Mitsuhashi and M. Nakatani, *Sens. Actuators, B*, 2014, **202**, 873.
13. A. Rivadeneyra, J. Fernández-Salmerón, M. Agudo-Acemel, J. A. López-Villanueva, A. J. Palma and L. F. Capitan-Vallvey, *Sens. Actuators, B*, 2015, **210**, 542.
14. Z. Dai, C.-S. Lee, Y. Tian, I.-D. Kimb and J.-H. Lee, *J. Mater. Chem. A*, 2015, **3**, 3372.
15. L. Li, S. He, M. Liu, C. Zhang and W. Chen, *Anal. Chem.*, 2015, **87**, 1638.
16. K. S. Kim, W. H. Baek, J. M. Kim, T. S. Yoon, H. H. Lee, C. J. Kang and Y. S. Kim, *Sensors*, 2010, **10**, 765.
17. S. Shao, M. Dimitrov, N. Guan and R. Köhn, *Nanoscale*, 2010, **2**, 2054.
18. X. Sun, X. Hu, Y. Wang, R. Xiong, X. Li, J. Liu, H. Ji, X. Li, S. Cai and C. Zheng, *The Journal of Physical Chemistry C*, 2015, **119**, 3228.
19. S. Shao, M. Dimitrov, N. Guan and R. Köhn, *Journal of Materials Chemistry*, 2009, **19**, 8411.
20. K. Galatsis, L. Cukrov, W. Wlodarski, P. McCormick, K. Kalantar-zadeh, E. Comini and G. Sberveglieri, *Sens. Actuators B*, 2003, **93**, 562.
21. H. Huang, H. Gong, C. L. Chow, J. Guo, T. J. White, M. S. Tse and O. K. Tan, *Adv. Funct. Mater.*, 2011, **21**, 2680.
22. Y. Liu, H. Zhang, Z. Zhang, Y. Xie and E. Xie, *Appl. Surf. Sci.*, 2010, **257**, 1236.
23. X. Xue, Z. Chen, C. Ma, L. Xing, Y. Chen, Y. Wang and T. Wang, *J. Phys. Chem. C*, 2010, **114**, 3968.
24. Y. C. Lee, Y. L. Chueh, C. H. Hsieh, M. T. Chang, L. J. Chou, Z. L. Wang, Y. W. Lan, C. D. Chen, H. Kurata and S. Isoda, *Small*, 2007, **3**, 1356.
25. J. X. Wang, X. W. Sun, Y. Yang and C. M. L. Wu, *Nanotechnology*, 2009, **20**, 465501.
26. C. Sinturel, M. Vayer, M. Morris and M. A. Hillmyer, *Macromolecules*, 2013, **46**, 5399.
27. M. N. Rumyantseva, A. M. Gaskov, N. Rosman, T. Pagnier and J. R. Morante, *Chem. Mater.*, 2005, **17**, 893.
28. Y. Liu, C. Zheng, W. Wang, C. Yin and G. Wang, *Adv. Mater.*, 2001, **13**, 1883.
29. J. X. Zhou, M. S. Zhang, J. M. Hong and Z. Yin, *Solid State Commun.* , 2006, **138**, 242.
30. A. Dieguez, A. Romano-Rodrıguez, A. Vila and J. R. Morante, *J. Appl. Phys.*, 2001, **90**, 1550.
31. T. Pagnier, M. Boulova, A. Galerie, A. Gaskov and G. Lucazeau, *Sens. Actuators, B*, 2000, **71**, 134.
32. X. Liu, N. Chen, B. Han, X. Xiao, G. Chen, I. Djerdj and Y. Wang, *Nanoscale*, 2015, **7**, 14872.
33. A. Gurlo, M. Sahm, A. Oprea, N. Barsan and U. Weimar, *Sens. Actuators B*, 2004, **102**, 291.
34. P. Clément, S. Korom, C. Struzzi, E. J. Parra, C. Bittencourt, P. Ballester and E. Llobet, *Advanced Functional Materials*, 2015, **25**, 4011.
35. J. H. Kim and S. S. Kim, *ACS Appl. Mater. Interfaces*, 2015, **7**, 17199.
36. A. Gurlo, Ba, N. rsan, A. Oprea, M. Sahm, T. Sahm and U. Weimar, *Appl. Phys. Lett.*, 2004, **85**, 2280.
37. S. Liu, F. Hu, J. Zhang, H. Tang and M. Shao, *ACS Appl. Mater. Interfaces*, 2013, **5**, 3208.
38. M. Yang, D. H. Kim, W. S. Kim, T. J. Kang, B. Y. Lee, S. Hong, Y. H. Kim and S. H. Hong, *Nanotechnology*, 2010, **21**, 215501.
39. M. Yang, H. C. Kim and S.-H. Hong, *Materials Letters*, 2012, **89**, 312.

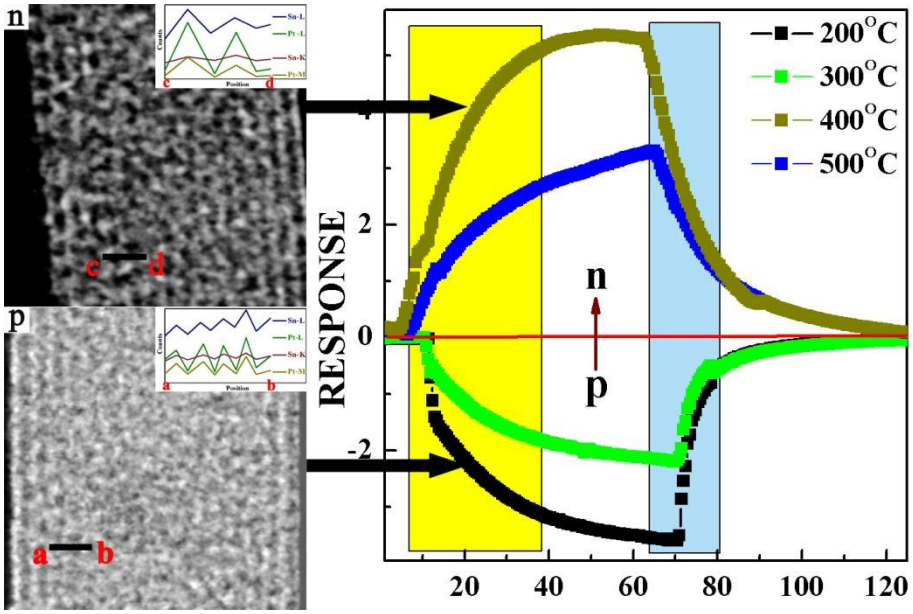

Gas sensing with ordered nanoporous materials is achieving much attention because of its promising capability of detecting toxic gases at room temperature. In this work, an ordered nanoporous SnO_2 sensing film is fabricated in situ on a sensing device using a block polymer template and is applied as a chemiresistive toluene gas sensor. The post synthetic hydrothermal treatment was developed for the synthesis of the ordered SnO_2 sensing films with homogeneous and controlled film thickness and the controllable pore size. The structure, crystallinity and composition of the ordered nanoporous SnO_2 thin films are characterized by HRTEM, FESEM, SAED, and STEM. Interestingly, the SnO_2 nanoporous film, an n-type material, presents tunable sensing behaviour with the switching from p- to n-type toluene sensing performance as a function of the platinum content and calcination temperature. The ordered nanporous sensing film is capable of detecting low levels of toluene, as low as 10 ppm, at room temperature, and shows good stability. Furthermore, a transition diagram has been created on the basis of the toluene sensing response, which can be used to design the p-n transitions.